

# Probing crossover from analogous weak antilocalization to localization by an Aharonov-Bohm interferometer on topological insulator surface

Zhen-Guo Fu,<sup>1,2</sup> Ping Zhang,<sup>2,\*</sup> and Shu-Shen Li<sup>1,†</sup>

*<sup>1</sup>State Key Laboratory for Superlattices and Microstructures,  
Institute of Semiconductors, Chinese Academy of Sciences,  
P. O. Box 912, Beijing 100083, People's Republic of China*

*<sup>2</sup>LCP, Institute of Applied Physics and Computational Mathematics,  
P.O. Box 8009, Beijing 100088, China*

## Abstract

We propose a scanning tunneling microscopy Aharonov-Bohm (AB) interferometer on the surface of a topological insulator (TI) to probe the crossover from analogous weak antilocalization (WAL) to weak localization (WL) phenomenon via the AB oscillations in spin-resolved local density of states (LDOS). Based on our analytical and numerical results, we show that with increasing the energy gap of TI surface states, the  $\Phi_0/2=hc/2e$  periodic AB oscillations in spin-resolved LDOS gradually transit into the  $\Phi_0$  periodic oscillations.

PACS numbers: 73.20.At, 73.23.-b, 74.55.+v, 71.70.Ej

---

\*zhang\_ping@iapcm.ac.cn

†sslee@semi.ac.cn

Topological insulators (TI) have attracted substantial interest in the modern condensed matter physics since their extraordinary edge and surface states [1, 2]. Following a series of theoretical predictions [3–6], a variety of two-dimensional [7] and three-dimensional [8–11] TI materials have been realized in recent experiments. The helical spin structure of Dirac electrons in the gapless strong TIs acquire a spin-orbit induced nontrivial Berry phase of  $\pi$  after a  $2\pi$  adiabatic rotation along the Fermi surface, which results in prohibition of backscattering and the weak antilocalization (WAL). The WAL effect in TIs has been measured by transport experiments [12–18]. Through gradually doping Cr magnetic elements in  $\text{Bi}_2\text{Se}_3$  to open and increase the Dirac electrons’s energy gap, most recently, the crossover from WAL to weak localization (WL) has been well observed [19], consistent with theoretical prediction [20].

Meanwhile, the surface scanning tunneling microscopy (STM) measurements have been extensively carried out to study the electronic properties and impurity scattering effects of TIs [1, 2, 21]. Compared to the conventional transport techniques that give the averaged signals, the STM has its own advantages in probing and even manipulating single-impurity and multiple-impurity scattering, from which the more precise quantum processes and mechanisms become possible to reveal. In particular, due to the nature of the single Dirac cone, no complicated intervalley scattering events happen on the TI surface, therefore, *in situ* designing of specific impurity configurations and mapping of their scattered electronic states can be harnessed to image extraordinary quantum properties of TI surfaces. Recently, we proposed a spin-dependent Aharonov-Bohm (AB) interferometer [22], which consists of a spin-polarized STM tip and two identical nonmagnetic impurities, to probe the unique spin-texture related quantum scattering behaviors on *gapless* TI surfaces. Using this interferometer, we have shown an interesting analogous WAL phenomenon reflected from  $\Phi_0/2$  periodic AB oscillations in the spin-resolved local density of states (LDOS), which is absent in the conventional metal surface systems.

In the present paper, we extend to consider the spin-dependent AB effect on *gapped* TI surfaces. If the Dirac fermions gain mass by coupling to a magnetic exchange field, a gap will be induced in the system, breaking time reversal symmetry in scattering amplitudes, and as a consequence scattering and transport properties for gapped and gapless systems should be significantly different, as witnessed by the above-mentioned WAL to WL crossover. Inspired by this idea, thus we study the effects of finite gap on the AB oscillations in spin-resolved

LDOS that we previously initiated. The AB oscillations in the real-space LDOS maps are arisen from the magnetic flux threaded through the time-reversed self-crossing loops (see Fig. 1). We find on one hand that the total LDOS exhibits the AB oscillation with a period of  $\Phi_0=hc/e$  in both gapless and gapped cases. On the other hand, while the spin-resolved LDOS shows  $\Phi_0/2$  periodic AB oscillations on the gapless TI surface, as we have reported before [22], however, with increasing the energy gap, the  $\Phi_0/2$  period of AB oscillations in spin-resolved LDOS gradually disappears and at the same time the  $\Phi_0$  period becomes clear. In other words, the crossover from analogous WAL to WL on TI surface can be well observed using our spin-dependent AB interferometer instead of the complicated low-temperature transport measurement. This crossover is consistent with the evolution of the Berry phase with increasing the TI surface-state gap.

The TI surface, on which two nonmagnetic impurities are adsorbed, is described by a low-energy effective Dirac Hamiltonian

$$H = H_0 + V(\mathbf{r}), \quad (1)$$

where

$$H_0 = \hbar v_f (k_x \sigma_y - k_y \sigma_x) + \Delta \sigma_z, \quad (2)$$

with  $v_f$  ( $\approx 4 \sim 5 \times 10^5$  m/s for  $\text{Bi}_2\text{Te}_3$ -family TIs as numerically used throughout this paper) being the Fermi velocity and  $2\Delta$  the energy gap of massive Dirac fermions, which is absent in the massless limit.

$$V(\mathbf{r}) = \sum_{i=1}^2 U_i \sigma_0 \delta(\mathbf{r} - \mathbf{r}_i) \quad (3)$$

denotes the potential of two impurities located at  $\mathbf{r}_1 = (-d/2, 0)$  and  $\mathbf{r}_2 = (d/2, 0)$  with  $U_i$  the potential scattering strength for scalar impurities.  $\sigma_0$  is the  $2 \times 2$  unit matrix.

The unperturbed real-space Green's function  $G_0(\mathbf{r} - \mathbf{r}', \omega)$  can be obtained from the Fourier transformation of  $G_0(\mathbf{k}, i\omega) = (i\omega - H_0)^{-1}$  in the  $k$ -space, which after a straightforward derivation is given by

$$G_0(\mathbf{r} - \mathbf{r}', \omega) = \frac{-i\omega}{(2\hbar v_f)^2} \left[ (1 + \Delta/\omega \sigma_z) H_0^{(1)}(z) - i(\hat{\boldsymbol{\rho}} \times \boldsymbol{\sigma}) \cdot \hat{\mathbf{z}} \sqrt{\delta_+ \delta_-} H_1^{(1)}(z) \right], \quad (4)$$

and

$$G_0(\mathbf{0}, \omega) = \frac{|\omega|}{2\pi} \text{diag}[\delta_+ f_0, \delta_- f_0] \quad (5)$$

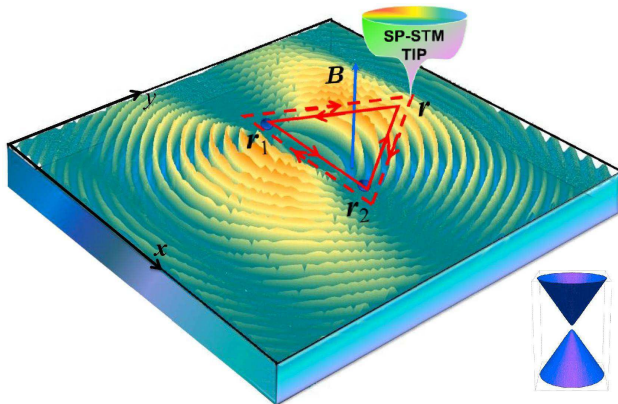


FIG. 1: (Color online) Surface electronic interferometer, comprising a spin polarized STM tip at  $\mathbf{r}$  and two impurities at  $\mathbf{r}_1$  and  $\mathbf{r}_2$  separately. The interference contributions in the LDOS is introduced by the electrons traveling along clockwise and anticlockwise loops enclosed by the STM tip and two impurities. The applied magnetic field  $B$  affects this interference via the AB effect.

for  $|\omega| > \Delta$ , where  $\delta_{\pm} = (1 \pm \Delta/\omega)$ ,  $z = \frac{\sqrt{\delta_{+}\delta_{-}\omega\rho}}{\hbar v_f}$  and  $f_0 = \int \frac{kdk}{\omega^2 - \Delta^2 - (\hbar v_f k)^2}$ . Here,  $\hat{\boldsymbol{\rho}}$  is the unit vector of  $\boldsymbol{\rho} = \mathbf{r} - \mathbf{r}'$  and  $H_{0/1}^{(1)}(z)$  are the Hankel functions of the first kind.

The features we discuss are expected to be seen in the change of the real-space LDOS owing to the influence of magnetic flux which passes through the area enclosed by the two scattering paths shown in Fig. 1. This quantity can reveal the analogous WL or WAL effect in TI via AB oscillatory periods in LDOS. The real-space Green's function involving the impurities scattering is given by Dyson equation  $G = G_0 + \delta G$ , with

$$\delta G = \int d\mathbf{r}'' G_0(\mathbf{r} - \mathbf{r}''; \omega) V(\mathbf{r}'') G(\mathbf{r}'', \mathbf{r}'; \omega). \quad (6)$$

Following the perturbation approach, Eq. (6) can be expanded to any order in the impurity potential  $V$ . Our effort is concentrated on the scattering processes of surface electrons with the both impurities, in which the scattering paths enclose loops [23]. Therefore, taking all this into account, after a long algebra calculation, we have

$$\begin{aligned} \delta G_L = & G_0(\mathbf{r} - \mathbf{r}_1) W_1 G_0(\mathbf{r}_1 - \mathbf{r}_2) T_2 G_0(\mathbf{r}_2 - \mathbf{r}') \\ & + G_0(\mathbf{r} - \mathbf{r}_2) W_2 G_0(\mathbf{r}_2 - \mathbf{r}_1) T_1 G_0(\mathbf{r}_1 - \mathbf{r}'), \end{aligned} \quad (7)$$

where the subscript  $L$  represents the loops enclosed by the scattering paths of the surface

electrons, and

$$W_i = \frac{T_i}{\sigma_0 - T_i G_0(\mathbf{r}_i - \mathbf{r}_j) T_j G_0(\mathbf{r}_i - \mathbf{r}_j)} \quad (8)$$

with  $T$ -matrices  $T_i = \frac{V_i}{\sigma_0 - V_i G_0(\mathbf{0}; \omega)}$  ( $i, j=1, 2$ ). Equation (7) is a general formula describing the two-impurity back and forth scattering of the STM-probed quasiparticles. Thus, the interference information during the time-reversal scattering processes are included in this equation.

In the presence of a weak magnetic field, the Green's function can be semiclassically approximated as

$$\tilde{G}_0(\mathbf{r} - \mathbf{r}', \omega) = e^{i \frac{2\pi}{\Phi_0} \int_{\mathbf{r}'}^{\mathbf{r}} \mathbf{A}(\mathbf{l}) \cdot d\mathbf{l}} G_0(\mathbf{r} - \mathbf{r}', \omega), \quad (9)$$

where  $\mathbf{A} = (-By, 0, 0)$  represents the vector potential. The correction of the LDOS due to the magnetic flux is given by

$$\begin{aligned} \Delta N_L(\mathbf{r}, \omega, B) &= -\frac{1}{\pi} \text{Im Tr} \left[ \delta \tilde{G}_L(\mathbf{r}, \omega) - \delta G_L(\mathbf{r}, \omega) \right] \\ &= \Delta N_L^\uparrow(\mathbf{r}, \omega, B) + \Delta N_L^\downarrow(\mathbf{r}, \omega, B), \end{aligned} \quad (10)$$

where  $\delta \tilde{G}_L$  is calculated from Eq. (7) with  $\tilde{G}_0$ . It is clear that the magnetic field affects the LDOS via the magnetic flux, which is easy to be obtained from the integral over the loops ( $\mathbf{r} \rightleftharpoons \mathbf{r}_1 \rightleftharpoons \mathbf{r}_2 \rightleftharpoons \mathbf{r}$ ),  $\oint_{\mathbf{l}} \mathbf{A}(\mathbf{l}) \cdot d\mathbf{l} = \pm B dy / 2 = \pm \Phi$ . In the present setup, we focus solely on the (spin-resolved) LDOS at  $\mathbf{r} = (x, y)$ , which is probed by the STM tip with the same plane coordinates. Since the STM tip also dually participate in composing the closed trajectory that the Dirac electron travels, hence under a fixed magnetic field  $B$ , the AB interference displays the oscillations with varying the tip position along the  $y$  direction.

The condition  $l_B > \lambda_f$  of the semiclassical approximation in Eq. (9) should be satisfied, here  $B=5$  T and  $\varepsilon_f=150$  meV are chosen from which the corresponding magnetic length  $l_B \approx 11.63$  nm while the Fermi wave length  $\lambda_f=10.5$  nm. Also, the Zeeman splitting by the external magnetic field is negligibly small (typically of 0.5 meV at  $B=5$  T for  $\text{Bi}_2\text{Se}_3$  film [24]) compared to the strong spin-orbit coupling (SOC), and thereby is neglected in this discussion. In a recent low temperature transport experiment [19] on magnetically doped  $\text{Bi}_2\text{Se}_3$  film, an energy gap as large as 100~300 meV near the Dirac point was observed, which is comparative with our choice in this work.

By choosing suitable Fermi energy  $\varepsilon_f$  and energy gap parameter  $\Delta$ , which can be controlled in experiments, the backscattering and the crossover from the WAL to WL can occur

on TI surface. When the Fermi energy lies in the gap, the interference signals arising from the contributions of  $\Delta N_L(\mathbf{r}, \omega, B=0)$  are so weak that the oscillatory ellipse features as well as the AB effect become ambiguous, hence we only consider  $\varepsilon_f > \Delta$ .

When the energy gap is opened, differing from the gapless case, the  $T$ -matrices  $T_i = \frac{V_i}{\sigma_0 - V_i G_0(\mathbf{0}; \omega)}$  ( $i, j=1, 2$ ) are not proportional to a unit matrix because  $G_0^{11}(\mathbf{0}; \omega) \neq G_0^{22}(\mathbf{0}; \omega)$ , thus the  $W_i$  matrices in Eq. (8) are no longer diagonal, resulting in intractable complexity in reducing Eq. (10). To get the asymptotic expression of LDOS we consider the lowest order in the impurity potential in Eq. (7), which is given by

$$\begin{aligned} \delta G_L^{(2)} &= U^2 \overline{G_0}(\mathbf{r} - \mathbf{r}_1) G_0(\mathbf{r}_1 - \mathbf{r}_2) G_0(\mathbf{r}_2 - \mathbf{r}') \\ &\quad + U^2 G_0(\mathbf{r} - \mathbf{r}_2) G_0(\mathbf{r}_2 - \mathbf{r}_1) G_0(\mathbf{r}_1 - \mathbf{r}'). \end{aligned} \quad (11)$$

For large distances ( $\omega\rho/\hbar v_f \gg 1$ ), the Hankel functions can be approximated as  $H_{0/1}^{(1)}(z) \approx \pm \sqrt{\frac{2}{\pi z}} e^{i(z \mp \pi/4)}$ , then the unperturbed Green's function has a simple asymptotic form

$$G_0(\mathbf{r} - \mathbf{r}') \approx \frac{-i\sqrt{\omega/2\pi\rho\hbar v_f}}{2\hbar v_f} \begin{pmatrix} \delta_+ e^{i(z - \frac{\pi}{4})} & \sqrt{\delta_+ \delta_-} e^{-i\vartheta} e^{i(z + \frac{\pi}{4})} \\ -\sqrt{\delta_+ \delta_-} e^{i\vartheta} e^{i(z + \frac{\pi}{4})} & \delta_- e^{i(z - \frac{\pi}{4})} \end{pmatrix}, \quad (12)$$

where  $e^{i\vartheta} = \frac{\rho \cdot (\hat{x} + i\hat{y})}{\rho}$ . Substituting this equation into Eq. (11) and after a tedious derivation, we obtain an explicit expression of the total LDOS as follows

$$\begin{aligned} \Delta N_L^{(2)}(\mathbf{r}, \omega, B) &\approx C \sin\left(\frac{\pi\Phi}{\Phi_0}\right) \left\{ (\delta_+^3 + \delta_-^3) \sin\left(\frac{\pi\Phi}{\Phi_0}\right) \right. \\ &\quad - \delta_+^2 \delta_- \left[ \sin\left(\frac{\pi\Phi}{\Phi_0} - \vartheta_1\right) + \sin\left(\frac{\pi\Phi}{\Phi_0} - \vartheta_2\right) + \sin\left(\frac{\pi\Phi}{\Phi_0} + 2\phi\right) \right] \\ &\quad \left. - \delta_-^2 \delta_+ \left[ \sin\left(\frac{\pi\Phi}{\Phi_0} + \vartheta_1\right) - \sin\left(\frac{\pi\Phi}{\Phi_0} - \vartheta_2\right) + \sin\left(\frac{\pi\Phi}{\Phi_0} - 2\phi\right) \right] \right\}, \end{aligned} \quad (13)$$

where  $C = 4U^2 (\omega/8\pi(\hbar v_f)^3)^{3/2} (1/\rho_1 \rho_2 d)^{1/2} \cos\left(\frac{\sqrt{\delta_+ \delta_-} \omega(\rho_1 + \rho_2 + d)}{\hbar v_f} - \frac{\pi}{4}\right)$ ,  $\phi = \frac{\vartheta_1 - \vartheta_2}{2}$  with  $e^{i\vartheta_{1/2}} = \frac{\rho_{1/2} \cdot (\hat{x} + i\hat{y})}{\rho_{1/2}}$  and  $\rho_{1/2} = \mathbf{r} - \mathbf{r}_{1/2}$ . The spin-up and spin-down LDOSs are written as

$$\begin{aligned} \Delta N_L^{(2)\uparrow/\downarrow}(\mathbf{r}, \omega, B) &\approx C \delta_{\pm} \sin\left(\frac{\pi\Phi}{\Phi_0}\right) \left\{ \delta_{\pm}^2 \sin\left(\frac{\pi\Phi}{\Phi_0}\right) - \delta_{\mp}^2 \sin\left(\frac{\pi\Phi}{\Phi_0} \mp 2\phi\right) \right. \\ &\quad \left. + \delta_+ \delta_- \left[ \sin\left(\frac{\pi\Phi}{\Phi_0} \pm \vartheta_2\right) - \sin\left(\frac{\pi\Phi}{\Phi_0} \mp \vartheta_1\right) \right] \right\}. \end{aligned} \quad (14)$$

Equations (13) and (14) are the main analytical result of this paper. Although the total and spin-resolved LDOSs are now explicitly obtained, their AB oscillation periods are still

difficult to analytically determine due to the weight coefficients  $\delta_+$  and  $\delta_-$  that arise from the energy gap. However, there exist two extreme cases: (i) One is the gapless limit where  $\delta_+=\delta_-=1$ ; (ii) The other one is the large-gap limit. For these two cases, one can further analytically simplify Eqs. (13) and (14) and get the periods of real-space AB oscillations in the LDOSs of TI.

The gapless case have been discussed in our last paper [22]. Actually, when  $\Delta=0$  we have the total LDOS quantity

$$\Delta N_L^{(2)}(\mathbf{r}, \omega, B) \Big|_{\Delta=0} \propto [\cos(2\pi\Phi/\Phi_0) - 1] \quad (15)$$

and its two spin compents

$$\Delta N_L^{(2)\uparrow/\downarrow}(\mathbf{r}, \omega, B) \Big|_{\Delta=0} \propto [\sin(2\pi\Phi/\Phi_0 \mp \phi) \pm \sin \phi]. \quad (16)$$

Obviously, the spacial AB oscillation period of the total LDOS is  $y_0 = \frac{2\Phi_0}{Bd}$  for fixed  $B$  and fixed impurity configuration, which corresponds to a  $\Phi_0$  period in the scale of flux.

As clearly seen from Eq. (16), comparing to the total LDOS, there occurs in the spin-resolved LDOS additional strong SOC induced quantum interference signature. This strong spin interference effect deviates the real-space AB oscillations from  $y_0$  period when a spin-polarized STM tip scans along the  $\hat{y}$ -direction on the TI surface in the presence of a fixed  $B$ . The AB interference period along the  $\hat{y}$ -direction can be numerically determined by solving the zero-point equation of the factors in Eq. (16), i.e.,  $\sin(\frac{2\pi\Phi}{\Phi_0} \mp \phi) \pm \sin \phi = 0$ . We can get the asymptotic roots  $y \approx \frac{n\Phi_0}{Bd}$  ( $n \in \mathbb{Z}$ ) for weak  $B$ . Therefore, the AB oscillation signals for  $\Delta N_L^{(2)\uparrow/\downarrow} \Big|_{\Delta=0}$  occur at  $\sim \frac{n\Phi_0}{Bd}$  with a spacial period of  $\frac{\Phi_0}{Bd} = \frac{a_0}{2}$  (i.e.,  $\frac{\Phi_0}{2}$  in the scale of flux), the half of  $\Delta N_L$ . This half period could be understood as an analog of WAL effect in the spin-resolved LDOS.

Turning to the other extreme case that the gap is large enough to be comparable with the Fermi energy  $\varepsilon_f$ . In this case, Eq. (14) is simplified to be

$$\begin{aligned} \Delta N_L^{(2)\uparrow}(\mathbf{r}, \omega, B) &\propto \delta_+^3 [\cos(2\pi\Phi/\Phi_0) - 1] \\ \Delta N_L^{(2)\downarrow}(\mathbf{r}, \omega, B) &\propto \delta_+^2 \delta_- [\cos(2\pi\Phi/\Phi_0) - 1] \end{aligned} \quad (17)$$

near the Fermi energy. Clearly, the spin-resolved LDOS  $\Delta N_L^{(2)\uparrow/\downarrow}$  turns now to display a complete  $\Phi_0$  period of AB oscillations as the total LDOS  $\Delta N_L^{(2)}$  does, which is totally different from the gapless case. In other words, the spin-resolved LDOS clearly exhibits

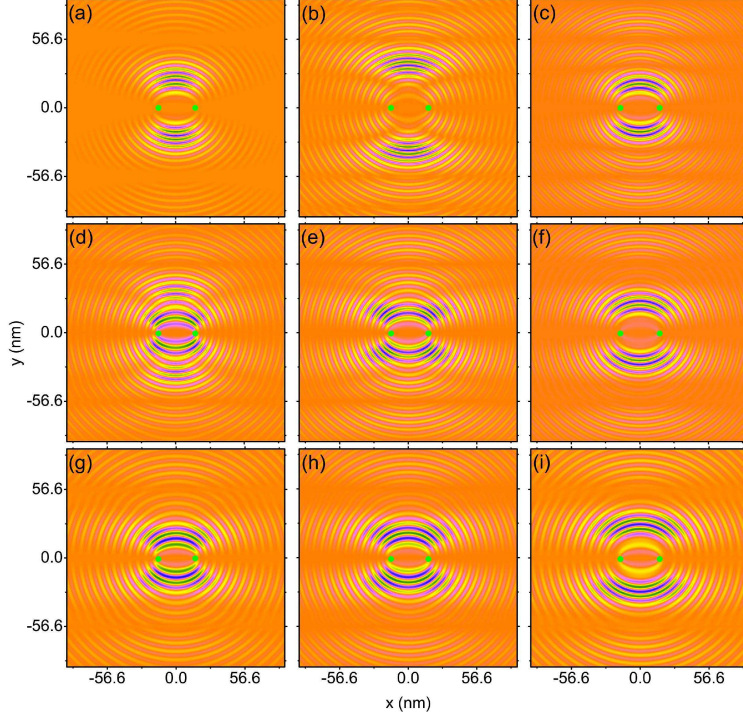


FIG. 2: (Color online) Simulations of the AB oscillations of the electronic LDOS in  $\text{Bi}_2\text{Te}_3(111)$  surface with two nonmagnetic impurities under a magnetic field  $B=5$  T. The left, middle, and right panels correspond to the total, spin-up, and spin-down LDOSs, respectively. We choose  $\Delta/\varepsilon_f=0$  in (a-c), 0.3 in (d-f), and 0.6 in (g-i) with  $\varepsilon_f=150$  meV. The horizontal strips in patterns are signature of AB effect. The green dots denote the impurity positions. The other parameters are chosen as  $v_f=4\times 10^5$  m/s,  $d=30$  nm, and  $U=1$  eV.

an analogous WL phenomenon in the large-gap limit. Except for these two extreme limits, to observe the AB oscillation period of spin-resolved LDOS for intermediate values of the energy gap, we resort to exact numerical analysis on original Eqs. (4-10).

From numerical calculations, we find by tuning the ratio of  $\Delta/\varepsilon_f$  that the crossover from half-period  $\Phi_0/2$  to period  $\Phi_0$  emerges in the AB oscillations of the spin-resolved LDOS. When  $\Delta/\varepsilon_f$  is small, the spacial AB oscillations of the spin-resolved LDOS still approximately possess a half period of  $\Phi_0/2$ , i.e., the analogous WAL effect is dominant in spin-resolved LDOS. However, with increasing  $\Delta/\varepsilon_f$ , the  $\Phi_0/2$  period of AB effect gradually disappears and at the same time the  $\Phi_0$  period becomes obvious in spin-resolved LDOS.

The typical numerical results are shown in Fig. 2 for different values of  $\Delta/\varepsilon_f$ . The

horizontal strips in each panel are the AB oscillation signals in the real-space LDOS. It is obvious that in the case of  $\Delta=0$ , the interstrip distance is  $y_0=\frac{2\Phi_0}{Bd}=56.6$  nm in the total LDOS as shown in Fig. 2(a), corresponding to the  $\Phi_0$  period of AB oscillations in total LDOS. Whereas, the interstrip distance becomes  $y_0/2=28.3$  nm in the spin-resolved LDOS as shown in Figs. 2(b) and 2(c), corresponding to the  $\frac{\Phi_0}{2}$  period of AB oscillations, which is consistent with the above analysis on Eq. (16). From Figs. 2(d-f) corresponding to  $\Delta/\varepsilon_f=0.3$ , we can observe that the horizontal strips in spin-resolved LDOSs patterns move towards the horizontal strips in total LDOS, signifying a crossover from analogous WAL to WL in the spin-resolved LDOS. With further increasing the ratio of  $\Delta/\varepsilon_f$ , the spin-resolved LDOS take on  $\Phi_0$  periodic AB oscillations, see the downmost panels (g-i) in Fig. 2 where  $\Delta/\varepsilon_f$  is chosen to be as large as 0.6. Much smaller values of  $B$  have also been tested in simulations, and the calculated AB oscillation patterns of (spin-resolved) LDOS are similar to those shown herein. Thus that, the AB effect can be effectively studied in a semiclassical way in a wide range of  $B$ .

Our findings can be understood from the view point of Berry phase. The TI surface Dirac electrons traveling along two time-reversed self-crossing loops ( $\mathbf{r}\Rightarrow\mathbf{r}_1\Rightarrow\mathbf{r}_2\Rightarrow\mathbf{r}$ ) differentiate by a Berry phase associated with spin rotation of  $2\pi$ , which is given by  $-i\int_0^{2\pi}d\theta_k\langle\psi_k|\partial_{\theta_k}|\psi_k\rangle=(1-\Delta/\varepsilon)\pi$ . Here, the eigenstates of  $H_0$  are expressed as  $|\psi_k\rangle=\frac{e^{i\mathbf{k}\cdot\mathbf{r}}}{\sqrt{2}}\left(\gamma_+, \mp i\gamma_-e^{i\theta_k}\right)^T$ , where  $\gamma_{\pm}=\sqrt{1\pm\Delta/\varepsilon}$ ,  $\tan\theta_k=k_y/k_x$ , and  $\varepsilon=\sqrt{(\hbar v_F k)^2+\Delta^2}$ . The two clockwise and anticlockwise loops enclosed by the STM tip and two impurities in Fig. 1 accumulate a Berry phase of  $\pi$  on a gapless TI surface due to the spin-momentum locking, and result in the WAL effect, which are represented as AB oscillations with half-period of  $\Phi_0/2$  in the spin-resolved LDOSs. While with the opening of the gap, the Berry phase departs from  $\pi$ . The larger ratio of  $\Delta/\varepsilon_f$  causes greater deviation of the Berry phase from  $\pi$ , leading to stronger WL tendency which is consistent with the observations from the AB interferometer proposed here. Therefore, the spin-dependent AB interferometer shown in this paper may provide a feasible approach to study the competition between WAL and WL by observing the spatial AB oscillation periods in the spin-resolved LDOS maps.

To experimentally verify our predictions exhibited here, the spin polarized STM technique is required, which we believe is achievable [25, 26]. Finally, we should point out that dephasing processes have been observed in transport investigations in  $\text{Bi}_2\text{Se}_3$  and  $\text{Bi}_2\text{Te}_3$

films [14, 17, 19] as well as in AB-effect studies of Bi<sub>2</sub>Se<sub>3</sub> nanowires [18]. The phase coherence length  $l_\phi$  of Bi<sub>2</sub>Se<sub>3</sub> and Bi<sub>2</sub>Te<sub>3</sub> can be as large as hundreds of nanometers, which is tens times of the Fermi wave length. The characteristic distance in our setup must be much smaller than the phase coherence length ( $d \ll l_\phi$ ), so that it is reasonable in Fig. 2 to choose  $d=30\text{nm} \ll l_\phi$  without taking into account the dephasing processes in the above numerical calculations.

In summary, we have performed a semiclassical analysis of the spin polarized STM probed AB oscillations in the LDOS induced by two impurities on a TI surface. With increasing the surface gap of TI, the crossover from analogous WAL to WL has been found in the AB oscillations of spin-resolved LDOS. This phenomenon may provide an important alternative approach to testify various extraordinary quantum wavefunction properties on the TI surface.

This work was supported by NSFC under Grants No. 90921003 and No. 60821061, and by the National Basic Research Program of China (973 Program) under Grants No. 2009CB929103 and No. G2009CB929300.

- 
- [1] M. Z. Hasan and C. L. Kane, Rev. Mod. Phys. **82**, 3045 (2010).
  - [2] X.-L. Qi and S.-C. Zhang, Rev. Mod. Phys. **83**, 1057 (2011).
  - [3] C. L. Kane and E. J. Mele, Phys. Rev. Lett. **95**, 226801 (2005).
  - [4] B. A. Bernevig, T. L. Hughes, and S.-C. Zhang, Science **314**, 1757 (2006).
  - [5] L. Fu, C. L. Kane, and E. J. Mele, Phys. Rev. Lett **98**, 106803 (2007).
  - [6] H. Zhang, C.-X. Liu, X.-L. Qi, X. Dai, Z. Fang, and S.-C. Zhang, Nature Phys. **5**, 438 (2009).
  - [7] M. König, S. Wiedmann, C. Brüne, A. Roth, H. Buhmann, L. W. Molenkamp, X.-L. Qi, S.-C. Zhang, Science **318**, 766 (2007).
  - [8] D. Hsieh, D. Qian, L. Wray, Y. Xia, Y. S. Hor, R. J. Cava, M. Z. Hasan, Nature **452**, 970 (2008).
  - [9] Y. L. Chen, J. G. Analytis, J.-H. Chu, Z. K. Liu, S.-K. Mo, X. L. Qi, H. J. Zhang, D. H. Lu, X. Dai, Z. Fang, I. R. Fisher, Z. Hussain, Z.-X. Shen, Science **325**, 178 (2009).
  - [10] Y. Xia, D. Qian, D. Hsieh, L. Wray, A. Pal, H. Lin, A. Bansil, D. Grauer, Y. S. Hor, R. J. Cava, and M. Z. Hasan, Nature Phys. **5**, 398 (2009).

- [11] D. Hsieh, Y. Xia, D. Qian, L. Wray, J. H. Dil, F. Meier, J. Osterwalder, L. Patthey, J. G. Checkelsky, N. P. Ong, A. V. Fedorov, H. Lin, A. Bansil, D. Grauer, Y. S. Hor, R. J. Cava, and M. Z. Hasan, *Nature* **460**, 1101 (2009).
- [12] E. B. Olshanetsky, Z. D. Kvon, G. M. Gusev, N. N. Mikhailov, S. A. Dvoretzky, and J. C. Portal, *JETP Lett.* **91**, 347 (2010).
- [13] P. Ghaemi, R. S. K. Mong, and J. E. Moore, *Phys. Rev. Lett.* **105**, 166603 (2010).
- [14] H.-T. He, G. Wang, T. Zhang, I.-K. Sou, G. K. L Wong, J.-N. Wang, H.-Z. Lu, S.-Q. Shen, and F.-C. Zhang, *Phys. Rev. Lett.* **106**, 166805 (2011).
- [15] J. Chen, H. J. Qin, F. Yang, J. Liu, T. Guan, F. M. Qu, G. H. Zhang, J. R. Shi, X. C. Xie, C. L. Yang, K. H. Wu, Y. Q. Li, and L. Lu, *Phys. Rev. Lett.* **105**, 176602 (2010).
- [16] M. Liu, C.-Z. Chang, Z. Zhang, Y. Zhang, W. Ruan, K. He, L. Wang, X. Chen, J.-F. Jia, S.-C. Zhang, Q.-K. Xue, X. Ma, and Y. Wang, *Phys. Rev. B* **83**, 165440, (2011).
- [17] J. Wang, Ashley M. DaSilva, C.-Z. Chang, K. He, J. K. Jain, N. Samarth, X.-C. Ma, Q.-K. Xue, M. H. W. Chan, *Phys. Rev. B* **83**, 245438 (2010).
- [18] H. Peng, K. Lai, D. Kong, S. Meister, Y. Chen, X.-L. Qi, S.-C. Zhang, Z.-X. Shen, and Y. Cui, *Nature Mater.* **9**, 225 (2010).
- [19] M. Liu, J. Zhang, C.-Z. Chang, Z. Zhang, X. Feng, K. Li, K. He, L. Wang, X. Chen, X. Dai, Z. Fang, Q.-K. Xue, X.-C. Ma, and Y. Wang, *Phys. Rev. Lett.* **108**, 036805 (2012).
- [20] H.-Z. Lu, J. Shi, and S.-Q. Shen, *Phys. Rev. Lett.* **107**, 076801 (2011).
- [21] R. R. Biswas and A. V. Balatsky, *Phys. Rev. B* **81**, 233405 (2010); R. R. Biswas and A. V. Balatsky, *ibid.* **83**, 075439 (2011).
- [22] Z.-G. Fu, P. Zhang, and S.-S. Li, *Appl. Phys. Lett.* **99**, 243110 (2011).
- [23] A. Cano and I. Paul, *Phys. Rev. B* **80**, 153401 (2009).
- [24] Z. Wang, Z.-G. Fu, S.-X. Wang, and P. Zhang, *Phys. Rev. B* **82**, 085429 (2010).
- [25] K. von Bergmann, M. Bode, A. Kubetzka, M. Heide, S. Blügel, and R. Wiesendanger, *Phys. Rev. Lett.* **92**, 046801 (2004).
- [26] S. Schmaus, A. Bagrets, Y. Nahas, T. K. Yamada, A. Bork, M. Bowen, E. Beaurepaire, F. Evers, and W. Wulfhekel, *Nature Nanotech.* **6**, 185 (2011).